Journal of the Korean Physical Society
https://doi.org/10.1007/s40042-023-00934-3

Online ISSN 1976-8524
Print ISSN 0374-4884

ORIGINAL PAPER - CONDENSED MATTER

First-principles study on the *d*-band center of Pt alloyed with 3*d* transition metals

Jeonghoon Hong[1,2] · **Sejoong Kim**[3,4] · **Jeongwoo Kim**[2,5]

Received: 18 July 2023 / Revised: 5 September 2023 / Accepted: 6 September 2023

Abstract

We study the catalytic activity properties of Pt doped and alloyed with 3*d* transition metal (Cr, Mn, and Fe). Using first-principles calculations, we investigate energetically favored configurations of doped Pt, including dopant locations in the Pt layers and distances between neighboring dopants. In a wide range of doping concentrations, our calculations on surface *d*-band centers reveal that the catalytic activity of the doped Pt is not considerably affected by transition metal impurities. In particular, Pt–Fe (1:1) alloys in an ordered face-centered tetragonal phase exhibit *d*-band centers aligned to the ideal value for the oxygen reduction reaction, which contrasts with disordered alloys whose *d*-band centers significantly deviate from the ideal one. This work suggests that doping and alloying Pt with transition metals is a promising route to design more affordable materials with lower Pt loading, while maintaining comparable to or even improved catalytic activity compared to pristine Pt.

Keywords First-principles calculation · Electronic structure · Density functional theory · Transition metal · Catalyst

1 Introduction

The oxygen reduction reaction (ORR) is a critical field of investigation due to its vital role in the cathodic process of proton exchange membrane fuel cells and metal–air batteries [1–7]. While noble platinum-based materials have been identified as highly efficient electro-catalysts for the ORR [8–10], their high cost and limited availability pose significant challenges to their practical application [1, 11]. The growing demand for fuel cell technology raises concerns about the long-term sustainability of Pt as a catalyst, given the limited reserves of this precious metal.

To address this issue, extensive research efforts have been directed toward developing a catalyst with lower Pt loading that exhibits similar or better ORR catalytic activity [12–15]. One effective approach is to enhance the surface area of Pt catalyst by reducing its size to nanoscale through nanoparticle dispersion [16]. In line with this strategy, investigations have extensively focused on incorporating Pt nanoparticles into carbon-based supports, such as carbon nanotubes or graphene [17–20]. These promising systems demonstrate the successful application of the nanoparticle dispersion method, leading to improved dispersion, increased surface area, and enhanced catalytic activity and durability [21].

Another promising approach is the alloying Pt with more affordable materials like Fe, Ni, Co, and Ti [22–25]. The utilization of composite catalysts with reduced Pt concentration has been found to exhibit even superior catalytic activity and performance for the ORR process [26, 27]. Therefore, it is imperative to understand the underlying mechanisms through which the enhanced performance of Pt catalysts is achieved when combined with nonprecious metals.

The *d*-band center of a catalyst is a widely accepted approach for predicting its catalytic activity in complex systems [28–30]. The efficiency of the ORR is primarily determined by the oxygen chemisorption energy. Metals with

✉ Sejoong Kim
sejoong@alum.mit.edu

✉ Jeongwoo Kim
kjwlou@inu.ac.kr

[1] Department of Physics, Indiana University, Bloomington, IN 47405, USA

[2] Department of Physics, Incheon National University, Incheon 22012, Korea

[3] University of Science and Technology (UST), Gajeong-Ro 217, Daejeon 34113, Korea

[4] Korea Institute for Advanced Study, Hoegiro 85, Seoul 02455, Korea

[5] Intelligent Sensor Convergence Research Center, Incheon National University, Incheon 22012, Korea

Published online: 18 October 2023

stronger oxygen bonding experience limited ORR efficiency due to the adsorbed O and OH species. Conversely, metals with weaker oxygen binding have their rate constrained either by the dissociation of O_2 or by the transfer of electrons and protons to adsorbed O_2 [31, 32]. The ORR activity is significantly influenced by the average energy level of the *d*-band states, as the positioning of *d*-band states in energy determines the chemical bonding between the catalyst and oxygen molecules. The close relationship between the catalyst and its *d*-band center has been investigated using X-ray photoelectron spectroscopy (XPS) and ultraviolet photoelectron spectroscopy (UPS) techniques [33, 34]. The ideal *d*-band center for the ORR reaction is estimated to be 0.2 eV lower than that of pure Pt [12, 13, 23, 35], enabling the search for materials with high catalytic activity using density functional theory calculations. Despite extensive scientific endeavors, pure Pt still exhibits the best catalytic efficiency among non-alloyed materials. Therefore, the surface electronic structure of Pt still needs intensive exploration to enhance the catalytic efficiency and design a practical catalyst without complex synthetic processes.

In this study, we investigate the variation in the *d*-band center of surface Pt in the presence of nonprecious metals using first-principles calculations. We study the energetically preferred configurations of 3*d* metal impurities in thin Pt (111) layers and evaluate their impact on the surface catalytic activity of Pt [36–38]. In addition, we calculate the *d*-band center for a highly ordered phase characterized by a high 3*d* metal concentration and compare it with that of a disordered phase exhibiting a random distribution of metal impurities. Our findings provide a practical guideline for the design of more efficient ORR catalysts with lower Pt content, thereby overcoming the limitations of traditional Pt-based catalysts.

2 Methods

We utilized the Vienna ab initio simulation package (VASP) [39] for our density functional theory (DFT) calculations using the projected augmented plane-wave method. The Perdew–Burke–Ernzerhof generalized gradient approximation was employed to account for the exchange–correlation functional [40, 41]. Our plane wave basis set had an energy cutoff of 400 eV, and we considered the self-consistent solution of the Kohn–Sham equations to be converged when the energy threshold reached below 10^{-5} eV. To sample the Brillouin zone, we employed a dense 7×7×1 k-point mesh. A vacuum distance of 20 Å perpendicular to the atomic plane was introduced to prevent interactions between layers. To ensure appropriate relaxation of the atomic structure and lattice parameters, we used a fully relaxed approach until the total energy was converged to below 10^{-4} eV. Our slab models consisted of six atomic layers, with each layer containing 4×4 in-plane unit cells, resulting in a total of 96 atoms. The *d*-band centers (ε_d) were calculated using the following formula:

$$\varepsilon_d = \frac{\int ED_{\mathrm{d}}(E - E_{\mathrm{f}})\mathrm{d}E}{\int D_{\mathrm{d}}(E - E_{\mathrm{f}})\mathrm{d}E},$$

where $D_{\mathrm{d}}(E)$ represents the density of states (DOS) for the *d*-orbital and E_{f} is the Fermi energy of the system. The integration ranges for all calculations were set from −10 eV to 5 eV. To estimate the surface *d*-band center, we calculated the average *d*-band center of the outermost Pt atoms, excluding the 3*d* metal atoms due to their low reactivity with oxygen molecules.

3 Results

We calculated the electronic structure of a six-layer Pt (111) surface (Fig. 1a). To examine the variation in the *d*-band center of Pt, we used a horizontally expanded (4×4) supercell. Figure 1b shows that the *d*-band center of Pt deviates from the bulk value at the surface, owing to the band bending caused by the surface potential [30, 42, 43]. While the surface layer has a higher *d*-band center with respect to the bulk value, the band center of inner-layers approaches the bulk value (indicated by the red horizontal line) as shown in Fig. 1b, which is comparable to one previously predicted [44]. The DOS of the outermost Pt layer is shifted slightly

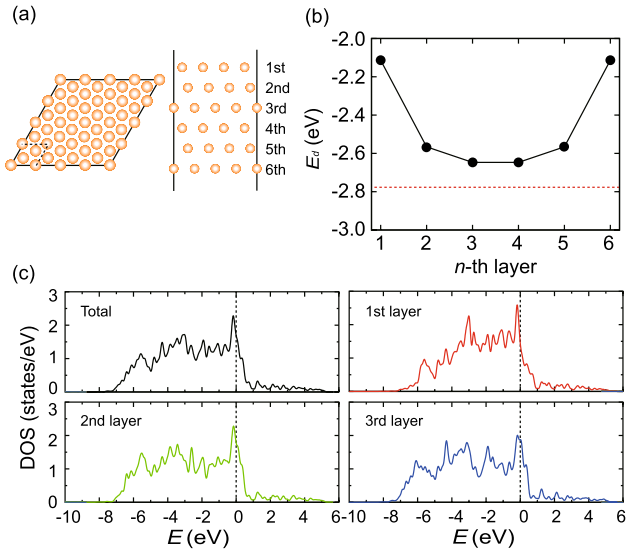

Fig. 1 **a** Top and side views of the atomic structure of a six-layer Pt (111) surface. **b** Calculated *d*-band center of each Pt layer in the Pt slab structure. The red horizontal line denotes the *d*-band center of bulk Pt. **c** Layer-resolved density of states (DOS) of the Pt surface. The Fermi level is set at zero energy

upward, while maintaining a similar overall shape. This suggests that the catalytic activity of Pt is likely related to the surface geometry-induced band.

We investigated the effect of 3*d* transition metal doping on the *d*-band center of the Pt surface for three different atoms (Cr, Mn, and Fe) in this study (Fig. 2a). For each atom, we analyzed the correlation between the vertical position of the impurity and the *d*-band center of the outermost layer (Fig. 2b). For all 3*d* metal doping cases (Fig. 2c), the outer layer dopant is energetically disfavored, indicating that dopants are more likely to be dispersed inside the Pt. The preference for the inner site is an important factor in utilizing nonprecious alloy as a pragmatic approach to enhance the economic feasibility of Pt catalyst [45]. When the 3*d* atoms are introduced to the Pt thin film, the *d*-band center of the outermost layer, a key determinant for catalytic reactions, is not significantly altered by the presence of the dopants (Fig. 2c), indicating the retention of the surface catalytic reactivity [46–49]. In particular, when dopants are located at the third layer, the *d*-band center of the surface layer is close to the pristine value because the dopants are spatially separated from the surface Pt. Therefore, the Pt alloying with 3*d* atoms provides a viable method to realize an economic fuel cell device without compromising the catalytic activity.

We also examined the effect of increasing 3*d* transition metal doping concentration on the variation of the *d*-band center of the surface Pt (Fig. 3a, b). Based on our finding of Fig. 2, the most energetically stable configuration with a dopant in the innermost layer, we conducted calculations

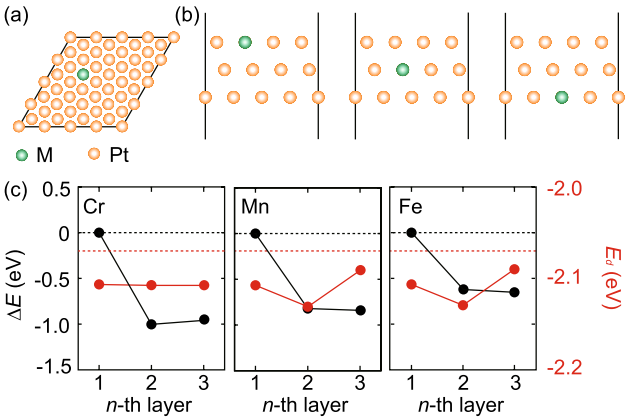

Fig. 2 **a** Top and **b** side views of the atomic structures of six-layer Pt (111) surfaces with a 3*d* transition metal impurity. The yellow and green spheres represent Pt and 3*d* transition metal (M) atoms, respectively. **c** The variation of the total energy of the Pt surface with a metal impurity (black lines) and the corresponding *d*-band center of the outermost Pt layer (red lines). The vertical position of the substituted atom is labeled as *n*th layer. The red horizontal dashed line represents the pristine *d*-band center value of the outermost Pt layer. The total energy is normalized to zero for the case where the dopant is located at the outermost layer

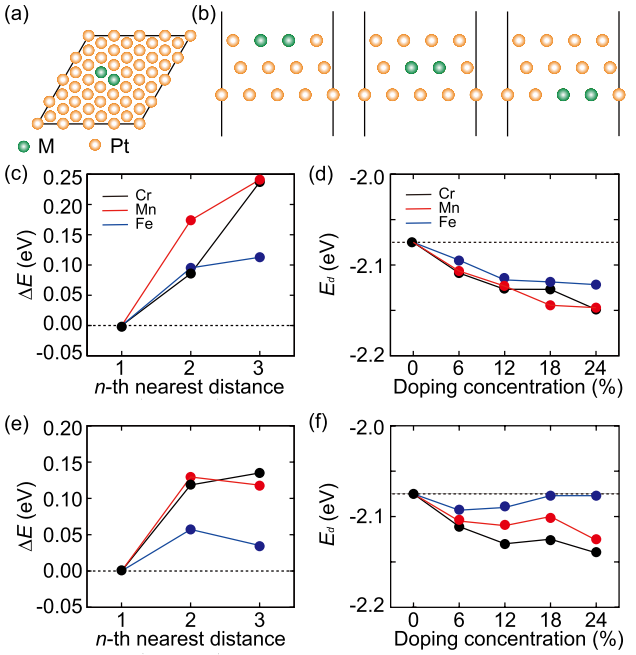

Fig. 3 **a** Top and **b** side views of the atomic structures of six-layer Pt (111) surfaces with 3*d* transition metal impurities on the same plane. The yellow and green spheres represent Pt and 3*d* transition metal (M) atoms, respectively. **c** The variation in the total energy (ΔE) of the Pt surface with 3*d* dopants upon the horizontal distance between the dopants on the third layer. ΔE is computed relative to the total energy for the case of the nearest neighboring dopant ($n=1$), represented by the solid dashed line. **d** Calculated *d*-band center of the outermost Pt layer depending on the doping concentration on the third layer. **e** ΔE of the Pt surface with 3*d* dopants upon the horizontal distance between the dopants on the first layer. **f** Calculated *d*-band center of the outermost Pt layer depending on the doping concentration on the first layer

to determine whether the dopants exhibit a preference for uniform dispersion or aggregation with neighboring dopants (Fig. 3c). The total energies of the Pt thin film are found to be the lowest when the transition metal atoms are adjacent to each other on the third layer, indicating that 3*d* dopants prefer to form clusters rather than disperse uniformly. Although the substituted metal atoms are not directly linked to the surface Pt layer, the *d*-band center of the outermost Pt is somewhat affected, indicating the importance of the core atomic/electronic structure of nano-sized Pt catalyst. The Pt *d*-band center monotonically decreases with the 3*d* metal concentration for Cr, Mn, and Fe dopants as shown in Fig. 3d.

Since surface doping affects the *d*-band center of the surface Pt layer most compared with the inner layer doping, we also investigated the dopant dispersion and the shift of the Pt *d*-band center by the surface 3*d* metals. As observed in the third layer doping, the 3*d* metals on the surface exhibit a similar propensity for clustering (Fig. 3e). Interestingly, for all cases considered, the *d*-band centers exhibit an upturn in the range of 6–15%, and the *d*-band centers of Fe-doped

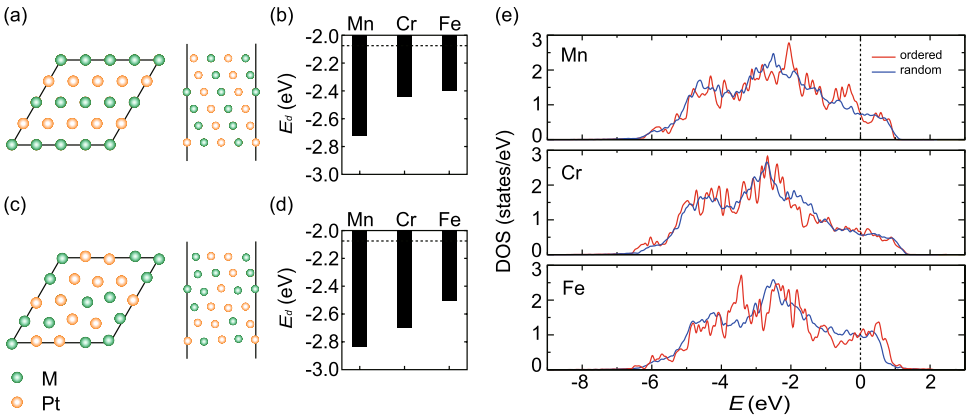

Fig. 4 Top and side views of Pt-metal (1:1) alloys in **a** an ordered face-centered tetragonal structure and **c** a disordered face-centered cubic one. Calculated *d*-band centers of the surface Pt layer for Pt–Mn, Pt–Cr, and Pt–Fe alloys in **b** ordered and **d** disordered phases. Black dotted lines denote the surface *d*-band center of pristine Pt. **e** Calculated density of states (DOS) of the outermost Pt layer for the Pt–Mn, Pt–Cr, and Pt–Fe alloys. The Fermi level is set at zero energy

Pt even recover the pristine value of Pt at higher doping concentrations (see Fig. 3f). As the doping concentration increases, there is a transformative shift in how the dopants and Pt interact. For doping concentrations up to 12%, the 3*d* atoms appear to mainly modulate the Pt matrix as isolated dopants, introducing slight modifications to the electronic structure of the Pt surface such as electron transfer. However, when we go beyond this threshold, the escalating presence of 3*d* dopants promotes the formation of metal clusters on the Pt surface. These emergent clusters are likely to have different interaction dynamics with the Pt substrate compared to their isolated counterparts, leading to the notable non-linear deviations seen in the *d*-band center.

Differing responses by elements such as Fe, as compared to Mn and Cr, might be attributed to their individual tendencies to cluster and their inherent electronic interactions with Pt. The significant atomic size difference between Pt and Cr leads to an additional strain effect, a well-known factor for controlling the *d*-band center [50]. Another important point is that Fe shares a similarity with Pt in terms of the number of valence electrons, resulting in a smaller difference in their Fermi levels. In contrast, when there's a larger disparity in the number of valence electrons, as seen between Pt and other elements, there tends to be a more substantial electron transfer in the *d*-orbitals. Therefore, an optimum doping concentration can be determined in Pt–Fe nanoparticles, minimizing the damages of the catalytic activity. The fact that the ideal *d*-band center for the ORR is ~ 0.2 eV lower than that of pure Pt [12, 13, 23, 35] provides a foundation for expecting improved reaction efficiency within the optimal alloying range.

Pt metal alloys can undergo a structural transition from a disordered face-centered cubic (FCC) phase to an ordered face-centered tetragonal (FCT) phase at high metal concentrations [51]. We investigated the effect of this phase transition on the catalytic activity of Pt alloys by calculating their *d*-band center. In the FCT phase, 3*d* transition metal atoms and Pt atoms are ordered in a line shape, as shown in Fig. 4a, resulting in a significant shift of the *d*-band center of the surface Pt layer, as illustrated in Fig. 4b. Fe alloying reduces the *d*-band center of the surface Pt by 0.3 eV, suggesting the FCT Pt–Fe alloy holds promise as a catalyst for the ORR. On the contrary, in the disordered FCC phase (Fig. 4c), the *d*-band center of the surface Pt in all the cases investigated in our calculations exhibits a substantial deviation from the ideal range for the ORR (Fig. 4d). Based on the result of the *d*-band adjustment achieved through 3*d* metal alloying, it can be concluded that the ordered structure is preferable for the ORR process compared to the disordered structure with a random distribution of 3*d* atoms.

We conducted an analysis on the DOS of the surface Pt layer to identify the noticeable change in the *d*-band center for the disordered phase, as shown in Fig. 4e. The primary disparity in the DOS between the ordered and disordered phases is that the DOS is comparatively smoother, accompanied by a prominent peak below − 4 eV, for the disordered structure. For example, in the Pt–Mn alloy, the peaks near the Fermi level are considerably reduced in the disordered phase. Similarly, the large peak near − 3.8 eV observed in the ordered Pt–Fe alloy disappears in the random phase. The broader shape of the DOS with reduced peak intensity indicates strong hybridization of the surface Pt atoms with their neighbors, leading to the splitting of the *d* bands into binding and antibonding states. This variation in the electronic structure of the surface Pt facilitates the shift of the *d*-band center toward lower energy levels.

4 Conclusion

We employed first-principles calculations to investigate the effect of nonprecious metal impurities on the *d*-band center of surface Pt. We analyzed the energetically preferred configurations of 3*d* metal impurities in thin Pt (111) layers by varying its vertical position and concentration. We demonstrated that 3*d* metal doping does not significantly impair the catalytic activity of the surface Pt layer. We also revealed that the ordered phase of Pt–Fe alloy, with an idea *d*-band center, is a more favorable candidate for the ORR compared to the random FCT phase. The strong binding induced by the random distribution of metal dopants is adverse to the manipulation of the *d*-band center of the surface Pt. Our results offer a fundamental understanding of how the *d*-band center of Pt can be controlled through the process of alloying it with more affordable metals.

Acknowledgements This work was supported by Incheon National University Research Grant in 2020 (2020-0371).

References

1. M.K. Debe, Nature **486**, 43 (2012)
2. D. Banham, S. Ye, ACS Energy Lett. **2**, 629 (2017)
3. X.X. Wang, M.T. Swihart, G. Wu, Nat. Catal. **2**, 578 (2019)
4. M. Shao, Q. Chang, J.-P. Dodelet, R. Chenitz, Chem. Rev. **116**, 3594 (2016)
5. Y.-C. Lu, Z. Xu, H.A. Gasteiger, S. Chen, K. Hamad-Schifferli, Y. Shao-Horn, J. Am. Chem. Soc. **132**, 12170 (2010)
6. S. Sui, X. Wang, X. Zhou, Y. Su, S. Riffat, C. Liu, J. Mater. Chem. A **5**, 1808 (2017)
7. S.J. Peighambardoust, S. Rowshanzamir, M. Amjadi, Int. J. Hydrogen Energy **35**, 9349 (2010)
8. V. Viswanathan, H.A. Hansen, J. Rossmeisl, J.K. Nørskov, ACS Catal. **2**, 1654 (2012)
9. V.R. Stamenkovic, B. Fowler, B.S. Mun, G. Wang, P.N. Ross, C.A. Lucas, N.M. Marković, Science **315**, 493 (2007)
10. J. Greeley, I.E.L. Stephens, A.S. Bondarenko, T.P. Johansson, H.A. Hansen, T.F. Jaramillo, J. Rossmeisl, I. Chorkendorff, J.K. Nørskov, Nat. Chem. **1**, 552 (2009)
11. M.A. Abbas, J.H. Bang, Chem. Mater. **27**, 7218 (2015)
12. F. Ando, T. Tanabe, T. Gunji, S. Kaneko, T. Takeda, T. Ohsaka, F. Matsumoto, A.C.S. Appl, Nano Mater. **1**, 2844 (2018)
13. F. Ando, T. Gunji, T. Tanabe, I. Fukano, H.D. Abruña, J. Wu, T. Ohsaka, F. Matsumoto, ACS Catal. **11**, 9317 (2021)
14. C. Wang, D. Van Der Vliet, K.L. More, N.J. Zaluzec, S. Peng, S. Sun, H. Daimon, G. Wang, J. Greeley, J. Pearson, A.P. Paulikas, G. Karapetrov, D. Strmcnik, N.M. Markovic, V.R. Stamenkovic, Nano Lett. **11**, 919 (2011)
15. J. Zhang, H. Yang, J. Fang, S. Zou, Nano Lett. **10**, 638 (2010)
16. M. Li, Z. Zhao, T. Cheng, A. Fortunelli, C.-Y. Chen, R. Yu, Q. Zhang, L. Gu, B.V. Merinov, Z. Lin, E. Zhu, T. Yu, Q. Jia, J. Guo, L. Zhang, W.A. Goddard, Y. Huang, X. Duan, Science **354**, 1414 (2016)
17. X. Ren, Y. Wang, A. Liu, Z. Zhang, Q. Lv, B. Liu, J. Mater. Chem. A **8**, 24284 (2020)
18. S. Xu, Y. Kim, J. Park, D. Higgins, S.-J. Shen, P. Schindler, D. Thian, J. Provine, J. Torgersen, T. Graf, T.D. Schladt, M. Orazov, B.H. Liu, T.F. Jaramillo, F.B. Prinz, Nat. Catal. **1**, 624 (2018)
19. A. Zadick, L. Dubau, N. Sergent, G. Berthomé, M. Chatenet, ACS Catal. **5**, 4819 (2015)
20. Y.-J. Wang, N. Zhao, B. Fang, H. Li, X.T. Bi, H. Wang, Chem. Rev. **115**, 3433 (2015)
21. J. Zhang, K. Sasaki, E. Sutter, R.R. Adzic, Science **315**, 220 (2007)
22. V. Stamenkovic, B.S. Mun, K.J.J. Mayrhofer, P.N. Ross, N.M. Markovic, J. Rossmeisl, J. Greeley, J.K. Nørskov, Angew. Chem. Int. Ed. **45**, 2897 (2006)
23. V.R. Stamenkovic, B.S. Mun, M. Arenz, K.J.J. Mayrhofer, C.A. Lucas, G. Wang, P.N. Ross, N.M. Markovic, Nat. Mater. **6**, 241 (2007)
24. S.-I. Choi, S. Xie, M. Shao, J.H. Odell, N. Lu, H.-C. Peng, L. Protsailo, S. Guerrero, J. Park, X. Xia, J. Wang, M.J. Kim, Y. Xia, Nano Lett. **13**, 3420 (2013)
25. D. Van Der Vliet, C. Wang, M. Debe, R. Atanasoski, N.M. Markovic, V.R. Stamenkovic, Electrochim. Acta **56**, 8695 (2011)
26. A. Kostuch, I.A. Rutkowska, B. Dembinska, A. Wadas, E. Negro, K. Vezzù, V. Di Noto, P.J. Kulesza, Molecules **26**, 5147 (2021)
27. N. Ranjbar Sahraie, J.P. Paraknowitsch, C. Göbel, A. Thomas, P. Strasser, J. Am. Chem. Soc. **136**, 14486 (2014)
28. B. Hammer, Y. Morikawa, J.K. Nørskov, Phys. Rev. Lett. **76**, 2141 (1996)
29. T. Bligaard, J.K. Nørskov, Electrochim. Acta **52**, 5512 (2007)
30. J.K. Nørskov, F. Abild-Pedersen, F. Studt, T. Bligaard, Proc. Natl. Acad. Sci. USA **108**, 937 (2011)
31. G.S. Karlberg, J. Rossmeisl, J.K. Nørskov, Phys. Chem. Chem. Phys. **9**, 5158 (2007)
32. J. Rossmeisl, A. Logadottir, J.K. Nørskov, Chem. Phys. **319**, 178 (2005)
33. T. Hofmann, T.H. Yu, M. Folse, L. Weinhardt, M. Bär, Y. Zhang, B.V. Merinov, D.J. Myers, W.A. Goddard, C. Heske, J. Phys. Chem. C **116**, 24016 (2012)
34. B.S. Mun, M. Watanabe, M. Rossi, V. Stamenkovic, N.M. Markovic, P.N. Ross, J. Chem. Phys. **123**, 204717 (2005)
35. F.H.B. Lima, J. Zhang, M.H. Shao, K. Sasaki, M.B. Vukmirovic, E.A. Ticianelli, R.R. Adzic, J. Phys. Chem. C **111**, 404 (2007)
36. A. Stroppa, K. Termentzidis, J. Paier, G. Kresse, J. Hafner, Phys. Rev. B **76**, 195440 (2007)
37. X. Qi, T. Yang, P. Li, Z. Wei, Nano Mater. Sci. S2589965121000313 (2021).
38. W. Yu, M.D. Porosoff, J.G. Chen, Chem. Rev. **112**, 5780 (2012)
39. G. Kresse, J. Furthmüller, Phys. Rev. B **54**, 11169 (1996)
40. P.E. Blöchl, Phys. Rev. B **50**, 17953 (1994)
41. G. Kresse, D. Joubert, Phys. Rev. B **59**, 1758 (1999)
42. J.R. Kitchin, J.K. Nørskov, M.A. Barteau, J.G. Chen, J. Chem. Phys. **120**, 10240 (2004)
43. Z. Zhang, J.T. Yates, Chem. Rev. **112**, 5520 (2012)
44. B. Hammer, J.K. Nørskov, Surf. Sci. **343**, 211 (1995)
45. U. Tylus, Q. Jia, K. Strickland, N. Ramaswamy, A. Serov, P. Atanassov, S. Mukerjee, J. Phys. Chem. C **118**, 8999 (2014)
46. K.J.J. Mayrhofer, B.B. Blizanac, M. Arenz, V.R. Stamenkovic, P.N. Ross, N.M. Markovic, J. Phys. Chem. B **109**, 14433 (2005)
47. G.A. Somorjai, A.M. Contreras, M. Montano, R.M. Rioux, Proc. Natl. Acad. Sci. USA **103**, 10577 (2006)
48. Z.W. Seh, J. Kibsgaard, C.F. Dickens, I. Chorkendorff, J.K. Nørskov, T.F. Jaramillo, Science **355**, eaad4998 (2017)
49. E. Skúlason, V. Tripkovic, M.E. Björketun, S. Gudmundsdóttir, G. Karlberg, J. Rossmeisl, T. Bligaard, H. Jónsson, J.K. Nørskov, J. Phys. Chem. C **114**, 18182 (2010)
50. S. Schnur, A. Groß, Phys. Rev. B **81**, 033402 (2010)

51. Y. Kim, H.E. Bae, D. Lee, J. Kim, E. Lee, S. Oh, J.-H. Jang, Y.-H. Cho, M. Karuppannan, Y.-E. Sung, T. Lim, O.J. Kwon, J. Power Sources **533**, 231378 (2022)